Advances in Symplectic Tracking for Robust Modeling of Nonlinear Integrable Optics

Chad Mitchell*, Robert Ryne, and Ji Qiang

Lawrence Berkeley National Laboratory,
Berkeley, CA 94720, USA
*E-mail: ChadMitchell@lbl.gov
http://atap.lbl.gov/

The Integrable Optics Test Accelerator (IOTA), currently under commissioning at Fermilab, is a novel storage ring designed in part to investigate the dynamics of beams with large transverse tune spread in the presence of a strongly nonlinear integrable lattice. [1,2] One motivation for this design is the strong dependence of the particle tunes on amplitude, which leads to a decoherence of transverse oscillation modes that may help to suppress the development of coherent space charge instabilities in an intense beam. We describe the implementation of new numerical tools in the code IMPACT-Z to facilitate robust modeling of nonlinear integrable optics with space charge in IOTA. Tracking within the unique 1.8 m magnetic insert is performed using a new representation of the nonlinear integrable potential in the complex plane, together with a second-order symplectic integrator based on Yoshida splitting. Space charge is treated using either a traditional quasistatic grid-based Poisson solve (with one of several possible boundary conditions) or using a new spectral solver that is symplectic (by design) on the N-particle phase space of the macroparticle system. Numerical applications to IOTA modeling are described.

Keywords: Integrable lattice; symplectic integrators; intense space charge.

1. Introduction

The Integrable Optics Test Accelerator (IOTA), currently under construction at Fermilab, is a novel storage ring designed in part to investigate the dynamics of beams with large transverse tune spread in the presence of a strongly nonlinear integrable lattice. [1] The lattice design [2,3] makes use of a 1.8 m-long nonlinear magnetic insert with an s-dependent transverse magnetic field that is shaped to generate bounded, regular (integrable) motion in the transverse plane for on-momentum particles. A primary goal of IOTA is to demonstrate that nonlinear tune shifts exceeding 0.25 can be achieved without significant degradation of the dynamic aperture. [2] The strong dependence of particle tunes on amplitude leads to a decoherence of transverse oscillation modes that may help to suppress the particle-core resonances primarily responsible for beam halo development in intense beams, [4] suggesting a possible strategy for the mitigation of particle losses in facilities operating near the Intensity Frontier.

Several challenges are associated with modeling accurately the beam dynamics in IOTA, including the strong intrinsic nonlinearity of the system, the complex structure of the fields within the nonlinear magnetic insert, the need for robust

2

long-term tracking with space charge over $\sim$10K turns or more (for investigation of beam stability and low-level particle losses), the absence of a detailed theoretical understanding of the interplay between space charge and nonlinear integrability, and the sensitivity of the integrability of the system to a variety of perturbative effects. A primary goal of this study was to implement tools within the code IMPACT-Z for modeling nonlinear integrable optics (with space charge) in IOTA while avoiding sources of non-symplectic numerical artifacts, preserving as far as possible the structure of the ring as an integrable or near-integrable Hamiltonian system.

The following section describes the structure of the nonlinear magnetic insert field and potentials, and their relationship to the integrability of motion. Section 3 describes the symplectic integration algorithm used for tracking within the nonlinear magnetic insert. Section 4 describes the algorithm used for symplectic multiparticle tracking with space charge. Section 5 describes two applications to numerical modeling of beam dynamics in IOTA. We conclude with a brief summary.

2. Analytical Treatment of the Nonlinear Integrable Potential

We summarize the structure of the nonlinear magnetic insert in the ideal limit[1] that the magnetic field is transverse and slowly varying with longitudinal position, $\partial_s B_x, \partial_s B_y \approx 0$. Detailed theoretical treatments are provided elsewhere,[1,5] as is a description of the physical magnet design.[6]

The 2D magnetic field within the nonlinear insert is given by $\vec{B} = \nabla \times \vec{A} = -\nabla\psi$, where the magnetic vector potential $\vec{A}$ and the magnetic scalar potential ψ at a longitudinal position s are most easily expressed in terms of the dimensionless quantities:

$$F = \frac{A_s + i\psi}{B\rho}, \qquad \zeta = \frac{x + iy}{c\sqrt{\beta(s)}}, \qquad \tilde{t} = \frac{\tau c^2}{\beta(s)}, \qquad (1)$$

using the complex function:[5]

$$F(\zeta) = \left(\frac{\tilde{t}\zeta}{\sqrt{1 - \zeta^2}}\right)\arcsin(\zeta).$$

Here $\beta = \beta_x = \beta_y$ is the betatron amplitude across the drift space that will contain the magnet, $B\rho$ is the magnetic rigidity, τ is a dimensionless parameter characterizing the strength of the magnet, and $c \neq 0$ [m$^{1/2}$] characterizes the length scale of the potentials in the transverse plane. Fig. 1 illustrates the function F, together with the associated magnetic field lines.

Since $\vec{A}_\perp = 0$ in this model, the single-particle Hamiltonian within the nonlinear magnetic insert takes the following form, taking the longitudinal coordinate s as the independent variable:

$$H(X, P_x, Y, P_y, T, P_t; s) = -\sqrt{1 - \frac{2P_t}{\beta_0} + P_t^2 - P_x^2 - P_y^2} - \frac{A_s}{B\rho} - \frac{P_t}{\beta_0}, \qquad (2)$$
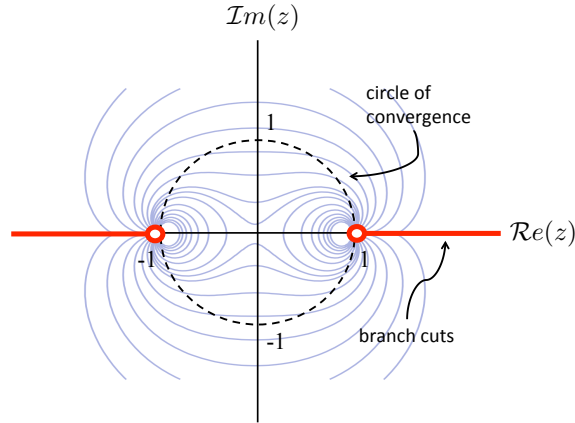
Fig. 1. Domain of analyticity of the complex function F, which defines the vector potential of the nonlinear insert in the transverse plane. The curves in blue denote magnetic field lines. The dashed circle denotes the circle of convergence of the multipole series. Singularities occur at the points $\zeta = \pm 1$.

where $P_x = p_x/p^0$ and $P_y = p_y/p^0$ are momenta normalized by the total design momentum p^0, β_0 is the relativistic beta of the reference particle, and $P_t = -\Delta\gamma/(\beta_0\gamma_0)$.

In the paraxial approximation $P_x, P_y << 1$, it follows that the Hamiltonian for an on-energy particle ($P_t = 0$) within the nonlinear magnetic insert takes the form:

$$H_\perp(X, P_x, Y, P_y; s) = \frac{1}{2}(P_x^2 + P_y^2) - \mathcal{Re}F(\zeta), \quad \zeta = \frac{X + iY}{c\sqrt{\beta(s)}}. \tag{3}$$

To see how (3) yields integrable motion, we perform an s-dependent transformation[1] to new phase space variables given by:

$$\begin{pmatrix} X_N \\ P_{xN} \end{pmatrix} = \begin{pmatrix} 1/c\sqrt{\beta} & 0 \\ \alpha/c\sqrt{\beta} & \sqrt{\beta}/c \end{pmatrix} \begin{pmatrix} X \\ P_x \end{pmatrix}, \qquad \begin{pmatrix} Y_N \\ P_{yN} \end{pmatrix} = \begin{pmatrix} 1/c\sqrt{\beta} & 0 \\ \alpha/c\sqrt{\beta} & \sqrt{\beta}/c \end{pmatrix} \begin{pmatrix} Y \\ P_y \end{pmatrix}. \tag{4}$$

Here $\alpha(s) = -\beta'(s)/2$, and the factors of c are included so that the normalized variables $(X_N, P_{xN}, Y_N, P_{yN})$ are dimensionless. Taking as the independent variable the betatron phase advance Ψ (defined by $\Psi' = 1/\beta$) within the drift containing the magnetic insert, the Hamiltonian corresponding to (3) in these normalized variables takes the dimensionless form:

$$H_N(X_N, P_{xN}, Y_N, P_{yN}; \Psi) = \frac{1}{2}(P_{xN}^2 + P_{yN}^2 + X_N^2 + Y_N^2) - \tau U(X_N, Y_N), \tag{5}$$

where

$$U = \mathcal{Re}\left(\frac{\zeta}{\sqrt{1-\zeta^2}} \arcsin(\zeta)\right), \qquad \zeta = X_N + iY_N. \tag{6}$$

4

Since H_N does not depend explicitly on the independent variable Ψ, H_N is an invariant of motion. The functional form of U is carefully chosen to yield a second invariant of motion, given by:

$$I_N = (X_N P_{yN} - Y_N P_{xN})^2 + P_{xN}^2 + X_N^2 - \tau W(X_N, Y_N), \quad W = \mathcal{R}e\left(\frac{\zeta + \zeta^*}{\sqrt{1 - \zeta^2}} \arcsin(\zeta)\right).$$

Here the star * denotes complex conjugation. It is not difficult to verify that $\{H_N, I_N\} = 0$, and that H_N and I_N are functionally independent, so it follows that (5) describes a completely integrable Hamiltonian system in the sense of Liouville.

In IOTA, the transfer map $\mathcal{R}$ for the remainder of the ring (from the exit of the nonlinear insert to its entrance), which we call the arc, is nearly linear with a net phase advance of $n\pi$ for some integer n. The map $\mathcal{R}$ is therefore described in normalized coordinates (4) by the matrix $\pm I$, where I is the 4×4 identity. It follows that H_N and I_N are each invariant under $\mathcal{R}$, and therefore under the one-turn map for the ring, so that the complete ring is described by an integrable symplectic one-turn map. Note, however, that integrability is ensured only when particles are on-energy in the paraxial approximation $P_x, P_y << 1$.

3. Symplectic Integrator and Implementation in IMPACT-Z

A new element type was added to the code IMPACT-Z to model the nonlinear magnetic insert described in the previous section. This element accepts as input the following 6 control parameters: L (insert length [m]), nSC (number of "space charge steps" across the insert), nMap (number of "map steps" per space charge step), τ (insert strength), c (scale parameter [m$^{1/2}$]), μ_0 (tune advance across the insert). An additional flag allows the user to select between tracking using the Hamiltonian (2) or using an approximate Hamiltonian obtained by expanding H through quadratic terms in the momenta.

Within this element, tracking with space charge is performed using a second-order symplectic integrator.[7–9] A two-level splitting of the Hamiltonian is used, where at each level we express the map over a longitudinal step of length h as:

$$H = H_1 + H_2, \qquad \mathcal{M}(h) = \mathcal{M}_1\left(\frac{h}{2}\right)\mathcal{M}_2(h)\mathcal{M}_1\left(\frac{h}{2}\right) + O(h^3), \tag{7}$$

where $\mathcal{M}_j$ is the symplectic map associated with the Hamiltonian H_j ($j = 1, 2$). Since H is in general non-autonomous, we must apply the following modification of (7), obtained by applying (7) to the corresponding map on the extended phase space:

$$\mathcal{M}(s \rightarrow s + h) = \mathcal{M}_1\left(s \rightarrow s + \frac{h}{2}\right)\mathcal{M}_2\left(h, s + \frac{h}{2}\right)\mathcal{M}_1\left(s + \frac{h}{2} \rightarrow s + h\right) + O(h^3).$$

Numerical evaluation is performed from left to right, where the map $\mathcal{M}_2$ appearing on the right-hand side is interpreted as the map generated by the Hamiltonian H_2

when the explicit appearance of the longitudinal coordinate is replaced by a fixed parameter equal to $s + h/2$.

The upper-level splitting, performed once per "space charge step," takes the form:[9]

$$H = H_{ext} + H_{SC}, \tag{8}$$

where H_{ext} is the Hamiltonian (2), and H_{SC} is an additional contribution due to space charge. The map $\mathcal{M}_{SC}$ is computed using techniques to be described in the following section.

Each "space charge step" is subdivided into nMap "map steps", for which we apply the lower-level splitting:

$$H_{ext} = H_{drift} + H_{NLL}, \tag{9}$$

where:

$$H_{drift} = -\sqrt{1 - \frac{2P_t}{\beta_0} + P_t^2 - P_x^2 - P_y^2} - \frac{P_t}{\beta_0} \quad \text{or} \quad H_{drift} = \frac{1}{2}(P_x^2 + P_y^2) + \frac{P_t^2}{2\beta_0^2\gamma_0^2},$$

and

$$H_{NLL} = -\mathcal{R}eF(\zeta), \qquad \zeta = \frac{X + iY}{c\sqrt{\beta(s)}}. \tag{10}$$

The maps $\mathcal{M}_{drift}$ and $\mathcal{M}_{NLL}$ are exactly known. In particular, if we define the quantities:

$$\mathcal{P} = P_x + iP_y, \qquad \sigma = \frac{h}{c\sqrt{\beta(s)}}, \tag{11}$$

the map $\mathcal{M}_{NLL}(h, s)$ affects only the momenta, taking $\mathcal{P} \rightarrow \mathcal{P}_f$ where:

$$\mathcal{P}_f = \mathcal{P} + \sigma \left(\frac{dF(\zeta)}{d\zeta} \right)^*. \tag{12}$$

Here the star denotes complex conjugation, and the derivative in (12) is exactly known. The map (12) is evaluated numerically using complex arithmetic.

Fig. 2 illustrates the scaling of numerical error with stepsize h obtained by tracking a single initial condition from the entrance of the nonlinear insert to its exit (a distance L). In each case, the quantities H_N and I_N are computed at the exit of the nonlinear insert and compared against the well-converged results obtained as $h \rightarrow 0$. The blue lines indicate the expected quadratic scaling of the global error. This second-order algorithm can easily be extended to fourth order (or higher) using the techniques of Yoshida.[8]
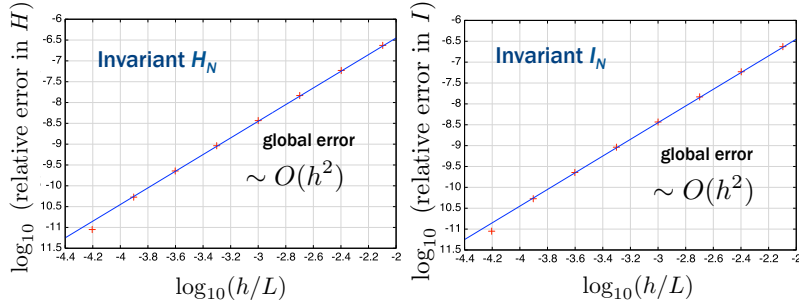
6

Fig. 2. Error in the quantities H_N and I_N at the exit of the nonlinear insert, obtained when tracking a single 2.5 MeV proton across the nonlinear insert with parameters $\tau = 0.45$, $c = 0.01$ m$^{1/2}$, $\mu_0 = 0.3$, and $L = 2.0$ m.

4. Implementation of a 2D Symplectic Spectral Space Charge Solver

Recently, there has been increased interest in the community in the development of algorithms for modeling collective self-field effects in plasmas and beams in a manner that preserves the Hamiltonian or symplectic structure of the collective multiparticle system.[10,11] This may be especially important for avoiding numerical artifacts during long-term tracking of intense beams in highly nonlinear systems such as IOTA. We describe the implementation of one such algorithm[11] within the code IMPACT-Z for modeling 2D space charge in an unbunched, coasting beam using a spectral method. For a system of N_p macroparticles with phase space coordinates $(\mathbf{r}_j, \mathbf{p}_j)$, $(j = 1, \ldots, N_p)$, the collective Hamiltonian of the system is expressed in the form:

$$H = \sum_{j=1}^{N_p} H_{ext}(\mathbf{r}_j, \mathbf{p}_j) + \frac{K}{2} \sum_{i=1}^{N_p} \sum_{j=1}^{N_p} G(\mathbf{r}_i, \mathbf{r}_j), \qquad (13)$$

where H_{ext} denotes the single-particle Hamiltonian including external fields,

$$K = \frac{qI}{2\pi\epsilon_0 p_0 v_0^2 \gamma_0^2} \qquad (14)$$

is the generalized perveance of the beam, and G is a Green function for the 2D Poisson equation with an appropriate boundary condition. Using the boundary condition for a rectangular conducting pipe (for simplicity), an approximation for G is obtained by using a finite number of Fourier modes in x and y as:

$$G(\mathbf{r}_i, \mathbf{r}_j) = 4\pi \frac{4}{ab} \frac{1}{N_p} \sum_{l=1}^{N_l} \sum_{m=1}^{N_m} \frac{1}{\gamma_{lm}^2} \sin(\alpha_l x_j)\sin(\beta_m y_j)\sin(\alpha_l x_i)\sin(\beta_m y_i) \qquad (15)$$

where

$$\alpha_l = \frac{l\pi}{a}, \quad \beta_m = \frac{m\pi}{b}, \quad \gamma_{lm}^2 = \alpha_l^2 + \beta_m^2. \qquad (16)$$

Here N_l, N_m are the number of Fourier modes and a, b are the aperture sizes in x and y, respectively.

At each longitudinal step, the splitting (7) may be applied to evaluate the map on the collective N_p-particle phase space. The map $\mathcal{M}_{SC}(h)$, corresponding to the second term in (13), affects only the particle momenta and is given by $\mathbf{p}_j \to \mathbf{p}_j^f$, $(j = 1, \ldots, N_p)$ where:

$$p_{x,i}^f = p_{x,i} - hK \sum_{j=1}^{N_p} \frac{\partial G(\mathbf{r}_i, \mathbf{r}_j)}{\partial x_i}, \quad p_{y,i}^f = p_{y,i} - hK \sum_{j=1}^{N_p} \frac{\partial G(\mathbf{r}_i, \mathbf{r}_j)}{\partial y_i}. \qquad (17)$$

Note that the momenta are normalized by the design momentum p^0, and that (17) is evaluated directly from the macroparticle coordinates in the laboratory frame. By grouping terms appropriately, the computational complexity of this algorithm scales as $O(N_{\mathrm{mode}} \times N_p)$, where $N_{\mathrm{mode}} = N_l N_m$ is the total number of modes. The algorithm is easily parallelized by distributing particles uniformly among computational cores.[11]

Figure 3 shows the result of a simple benchmark performed within IMPACT-Z. A coasting, uniform cylinder beam is initialized with zero momentum spread, and allowed to expand under its own space charge over the distance required to double in radius. For a coasting beam, the collective Hamiltonian (13) has no explicit dependence on the independent variable, and is therefore invariant under the continuous-time evolution of the N_p-particle system. Due to the use of numerical integration, which makes use of the Hamiltonian splitting (7), this quantity is numerically preserved within a global error that is second order in the stepsize h, as expected.
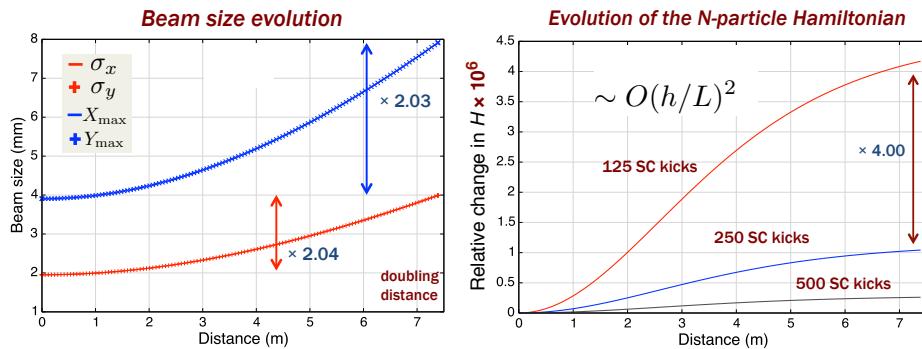

Fig. 3.   Simulation of a 2.5 MeV proton beam with 4.113 mA current and initial radius 3.9 mm expanding in free space ($a = b = 5$ cm) using $N_p = 1.024$ M. (a) Evolution of rms and total beam sizes. (b) The collective Hamiltonian given by (13,15). Note that $L \approx 7.4$ m.

8

5. Applications to IOTA modeling

As one application of these tools, we studied how non-ideal nonlinear effects in the arc, such as kinematic nonlinear effects and 2nd/3rd-order dipole effects, affect the preservation of the invariants H_N and I_N in the IOTA ring. A matched particle distribution representing a 2.5 MeV proton beam was initialized at the entrance to the nonlinear magnetic insert in the normalized coordinates $(X_N, P_{xN}, Y_N, P_{yN})$ according to the distribution function:[4]

$$f \sim \delta(H_N - \epsilon_0). \tag{18}$$

Here H_N is given in (5) and ϵ_0 denotes a generalized emittance characterizing the size of the beam in the 4D phase space. (It is convenient to normalize H_N by the quantity c^2, so that ϵ_0 has units of emittance. Here $\epsilon_0 = 4$ mm-mrad.) The beam is given zero energy spread. Figure 4 illustrates the evolution of $\sigma_{H_N}/\langle H_N \rangle$, evaluated at the midpoint of the nonlinear insert, over 8000 turns in the absence of space charge. When linear symplectic tracking is used within the lattice elements external to the nonlinear magnetic insert (blue), this quantity remains nearly zero, indicating the H_N is well-preserved, as expected from the theory of Section 2 and the linear optics of the IOTA lattice design. The green curve is obtained by using linear tracking within lattice elements (bends and quads) external to the nonlinear magnetic insert, except for the drift elements, which are treated exactly using the leftmost Hamiltonian following (9). Due to kinematic nonlinearities within the drift Hamiltonian, the invariants are no longer exactly preserved, although the degree of violation is quite small. The red curve is obtained after including 2nd and 3rd-order nonlinear effects within the dipoles, which are treated using symplectic Lie-algebraic map techniques.[12] The linear growth evident after turn 1000 suggests the presence of stochastic diffusion due to the breakup of invariant tori. Fig. 4(b) illustrates the scaling of this effect with the initial value of the generalized beam emittance ϵ_0. As expected, the effect becomes stronger as the initial beam emittance is increased, as the beam samples a larger region of the phase space affected by these nonlinearities.

As a second application, we studied the effect of weak space charge on the preservation of the invariants H_N and I_N using a version of the IOTA lattice designed for a current of 0.411 mA (a space charge tune shift of $\Delta Q = 0.03$). The lattice quadrupole settings were retuned[13] to restore nearly integer tune advance across the arc. Space charge is treated throughout the ring using the symplectic spectral space charge algorithm described in Section 4. For propagation in the external fields we use linear tracking for all elements external to the nonlinear magnetic insert (the "arc") to isolate the effect of space charge on the integrability of motion. The particle distribution is initialized according to the waterbag-like distribution function:

$$f \sim \Theta(H_N - \epsilon_0), \qquad \Theta(x) = \begin{cases} 1, & x \leq 0 \\ 0, & x > 0 \end{cases}. \tag{19}$$
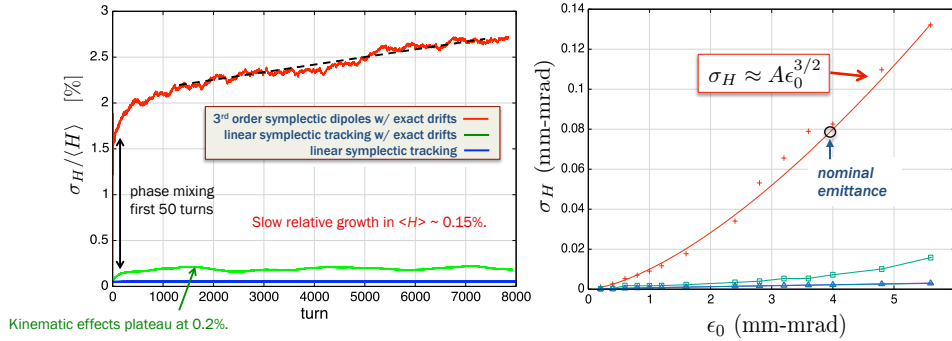
Fig. 4.   (a) Diffusion of the first invariant of motion produced by kinematic nonlinearities and 2nd-3rd order dipole effects. Initially, $\sigma_H \approx 0$. Note the rapid initial jump followed by linear growth. The corresponding value of $\sigma_I/\langle I \rangle$ grows by 1% over 8000 turns. (b) Simulations using several values of ϵ_0 suggest that $\sigma_H/\langle H \rangle \sim \sqrt{\epsilon_0}$.

Figure 5 illustrates the relative growth in the spread of the two invariants within the beam as a function of turn number. Here, we use $\sqrt{I_N}$ rather than I_N for practical reasons related to numerical benchmarking. In Figs. 5(a) and (b), we see behavior qualitatively similar to Fig. 4(a). This suggests that space charge may induce stochastic diffusion due to the breakup of invariant tori, but before drawing this conclusion it is important to understand the contributions of macroparticle noise and other numerical effects in detail. Other studies exploring the interplay between space charge, numerical noise, and integrability in IOTA have been described elsewhere. [14]
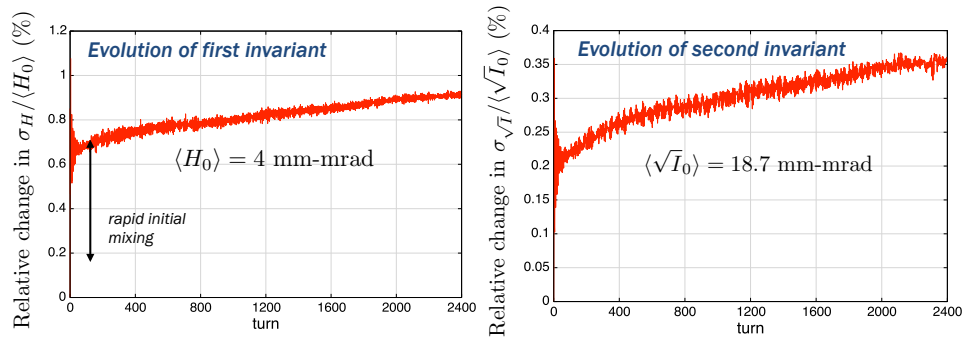

Fig. 5.   Illustration of space-charge induced diffusion of the two invariants of motion for $\Delta Q = 0.03$. (a) Diffusion of the first invariant of motion produced by space charge. Note the rapid initial jump in σ_H followed by slow linear growth. (b) Diffusion of the second invariant of motion produced by space charge.

10

6. Conclusions

A variety of new numerical tools have been implemented in the code IMPACT-Z to facilitate the modeling of nonlinear integrable optics in IOTA with space charge. A treatment of the nonlinear integrable potential of the IOTA magnetic insert in the complex plane is used as an alternative to[1] for numerical tracking, avoiding a previously problematic numerical instability. This is performed using a second-order symplectic integrator based on Yoshida splitting. Space charge can be treated using either a traditional grid-based Poisson solve (with a variety of possible boundary conditions) or using a new spectral solver that is symplectic (by design) on the N-particle phase space of the macroparticle system.[11] Simulations indicate slow diffusion of the invariants of motion in the presence of dipole nonlinearities or space charge. Future work will investigate in more detail the sensitivity of diffusion rates for the invariants of motion in IOTA to numerical artifacts that may be affected by the choice of Poisson solver and parameters such as the number of macroparticles, number of grid cells or spectral modes, and number of time steps.

Acknowledgments

References

1. V. Danilov and S. Nagaitsev, "Nonlinear Accelerator Lattices with One and Two Analytic Invariants," Phys. Rev. ST Accel. Beams **13**, 084002 (2010).
2. S. Nagaitsev *et al*, "Design and Simulation of IOTA - A Novel Concept of Integrable Optics Test Accelerator", in Proc. IPAC2012, New Orleans, LA, MOYCP01 (2012).
3. S. Antipov *et al*, "IOTA (Integrable Optics Test Accelerator): Facility and Experimental Beam Physics Program," Journal of Instrumentation **12**, T03002 (2017).
4. S. Webb *al*, "Suppressing Transverse Beam Halo with Nonlinear Magnetic Fields", in Proc. IPAC2013, Shanghai, China, p. 3099 (2013); FERMILAB-PUB-294-AD-APC (2012).
5. C. Mitchell, "Complex Representation of Potentials and Fields for the Nonlinear Magnetic Insert of the Integrable Optics Test Accelerators," LBNL Report LBNL-1007217 (2017).
6. F. O'Shea *et al*, "Measurement of Non-Linear Insert Magnets," in Proc. PAC2013, Pasadena, CA, p. 922 (2013).
7. R. Ruth, "A Canonical Integration Technique," IEEE Trans. Nucl. Sci. **30**, 4 (1983).
8. H. Yoshida, "Construction of Higher Order Symplectic Integrators," Physics Letters A **150**, 5 (1990).
9. J. Qiang *et al*, "An Object-Oriented Parallel Particle-in-Cell Code for Beam Dynamics Simulation in Linear Accelerators," J. Comp. Phys. **163**, 434-451 (2000).
10. S. Webb, "A Spectral Canonical Electrostatic Algorithm," Plasma Phys. Control. Fusion **58**, 034007 (2016).

11. J. Qiang, "Symplectic Multiparticle Tracking Model for Self-Consistent Space-Charge Simulation," Phys. Rev. ST Accel. Beams **20**, 014203 (2017).
12. A. J. Dragt, *Lie Methods for Nonlinear Dynamics with Applications to Accelerator Physics*, University of Maryland (2011).
13. A. Romanov *et al*, "Adaptive Matching of the IOTA Ring Linear Optics for Space Charge Compensation," NAPAC2016, Chicago, IL, p. 1152 (2016).
14. C. Hall *et al*, "Impact of Space Charge on Beam Dynamics and Integrability in the IOTA Ring," NAPAC2016, (slides) WEA4CO02, Chicago, IL, p. 1152 (2016).